Langmuir
Article
pubs.acs.org/Langmuir

Self-Patterned Mixed Phospholipid Monolayers for the Spatially Selective Deposition of Metals

Nathalie Y-Wa Tang and Antonella Badia*

Department of Chemistry, Université de Montréal, C.P. 6128, succursale Centre-ville, Quebec H3C 3J7, Canada, and FQRNT Center for Self-Assembled Chemical Structures (CSACS)

Received June 11, 2010. Revised Manuscript Received August 9, 2010

Metal-reactive organosulfur groups were patterned onto mica and silicon surfaces by dewetting instabilities during the Langmuir−Blodgett (LB) deposition of phase-separated mixed phospholipid monolayers. Monolayers were formed from binary mixtures of dipalmitoylphosphatidylcholine (DPPC), dilauroylphosphatidylcholine (DLPC), and their ω-methyldisulfide-dialkylphosphatidylcholine analogues, DSDPPC and DSDLPC. Patterns of highly parallel stripes of condensed DPPC or DSDPPC, protruding by 0.7−0.9 nm from a fluid matrix of DLPC or DSDLPC, were observed over areas extending at least $30 \times 30\ \mu m^2$ in the LB films. The average stripe width varied from ca. 150 to 500 nm, depending on the lipid composition and deposition pressure. X-ray photoelectron spectroscopy confirmed that the phospholipid-monolayer-bound methydisulfides react with Au vapor to form a gold−thiolate species. The adsorption of thermally evaporated Au, Ag, and Cu onto DSDPPC/DLPC and DPPC/DSDLPC patterns was investigated by field emission gun scanning electron microscopy (FEGSEM) and atomic force microscopy (AFM). A change in phase contrast is observed in FEGSEM and AFM over the methyldisulfide-functionalized areas following metal deposition due to metal−thiolate bond formation. An increase in step height between the DSDPPC stripes and nonfunctionalized DLPC background following metal deposition, as well as the resistance of the metal-coated DSDPPC or DSDLPC regions to detergent extraction from the surface, attest to a selective metallization of the pattern. Our results indicate that the preferential adsorption of vapor-deposited metal onto the ω-methyldisulfide-terminated phase occurs at submonolayer coverages. The chemical reactivity exhibited by the organosulfur-modified phospholipid LB films make these templates potentially interesting for the fabrication of solid-supported patterns of metal nanostructures.

Introduction

A variety of lithography-free surface patterning methodologies involving large-scale self-assembly have been developed over the past two decades to circumvent some limitations of photolithography and scanning beam lithography (i.e., accessibility, cost, low throughput, size of area patterned, or minimum feature size).[1,2] One approach is based on Langmuir−Blodgett (LB) technology, which is a well-established "bottom-up" method for preparing (ultra)thin films that are highly structured in the vertical and/or lateral directions.[3−7] It enables the deposition of monolayers of amphiphilic materials over macroscopic substrate areas (typically several square centimeters), control of the deposited film thickness and molecular density, and the buildup of multilayer structures with varying layer composition.[8] These general features and an easy-to-use inexpensive apparatus make LB technology appealing for micro- and nanofabrication.

Several reports have demonstrated the potential of the LB technique for preparing solid-supported films that are chemically or physically differentiated on the micrometer to submicrometer scale. Laterally patterned LB films are typically generated by the transfer onto substrates of two-dimensional arrays of domains formed at the air/water (A/W) interface by the pressure-induced, lateral phase separation of immiscible molecules or units, such as amphiphilic diblock copolymers[9−11] and mixtures of long-chain fatty acids[12−14] or lipids.[15−17] Alternatively, the vertical transfer process itself can produce a regular surface pattern from a homogeneous monolayer precusor.[5,7] The latter type of LB patterning results from oscillations of the water meniscus height on the withdrawing substrate that are triggered by solid surface-mediated changes in the molecular density or composition of the monolayer film at the three-phase contact line (air/aqueous subphase/solid substrate).[18−25] These oscillations switch the

*To whom correspondence should be addressed. E-mail: antonella.badia@umontreal.ca.

(1) Gates, B. D.; Xu, Q.; Love, J. C.; Wolfe, D. B.; Whitesides, G. M. *Annu. Rev. Mater. Res.* **2004**, *34*, 339.
(2) Gates, B. D.; Xu, Q.; Stewart, M.; Ryan, D.; Willson, C. G.; Whitesides, G. M. *Chem. Rev.* **2005**, *105*, 1171.
(3) Motschmann, H.; Möhwald, H. Langmuir-Blodgett Films. In *Handbook of Applied Surface and Colloid Chemistry*; Holmberg, K., Ed.; John Wiley & Sons, Ltd: New York, 2001; p 629.
(4) Lenhert, S.; Li, Z.; Mueller, J.; Wiesmann, H. P.; Erker, G.; Fuchs, H.; Chi, L. *Adv. Mater.* **2004**, *16*, 619.
(5) Chen, X.; Lenhert, S.; Hirtz, M.; Lu, N.; Fuchs, H.; Chi, L. *Acc. Chem. Res.* **2007**, *40*, 393.
(6) Tao, A. R.; Huang, J.; Yang, P. *Acc. Chem. Res.* **2008**, *41*, 1662.
(7) Badia, A.; Moraille, P.; Tang, N. Y. W.; Randlett, M.-E. *Int. J. Nanotechnol.* **2008**, *5*, 1371.
(8) Petty, M. C. *Langmuir-Blodgett Films. An Introduction*; Cambridge University Press: Cambridge, 1996.
(9) Zhu, J.; Eisenberg, A.; Lennox, R. B. *J. Am. Chem. Soc.* **1991**, *113*, 5583.
(10) Cox, J. K.; Yu, K.; Constantine, B.; Eisenberg, A.; Lennox, R. B. *Langmuir* **1999**, *15*, 7714.
(11) Lu, Q.; Bazuin, C. G. *Nano Lett.* **2005**, *5*, 1309.
(12) Overney, R. M.; Meyer, E.; Frommer, J.; Guentherodt, H. J.; Fujihira, M.; Takano, H.; Gotoh, Y. *Langmuir* **1994**, *10*, 1281.
(13) Qaqish, S. E.; Paige, M. F. *Langmuir* **2007**, *23*, 10088.
(14) Kimura, H.; Watanabe, S.; Shibata, H.; Azumi, R.; Sakai, H.; Abe, M.; Matsumoto, M. *J. Phys. Chem. B* **2008**, *112*, 15313.
(15) Seul, M.; Chen, V. S. *Phys. Rev. Lett.* **1993**, *70*, 1658.
(16) Dufrêne, Y. F.; Barger, W. R.; Green, J.-B. D.; Lee, G. U. *Langmuir* **1997**, *13*, 4779.
(17) Sanchez, J.; Badia, A. *Chem. Phys. Lipids* **2008**, *152*, 24.
(18) Graf, K.; Riegler, H. *Colloids Surf., A* **1998**, *131*, 215.
(19) Kovalchuk, V. I.; Bondarenko, M. P.; Zholkovskiy, E. K.; Vollhardt, D. *J. Phys. Chem. B* **2003**, *107*, 3486.
(20) Lenhert, S.; Gleiche, M.; Fuchs, H.; Chi, L. *ChemPhysChem* **2005**, *6*, 2495.
(21) Riegler, H.; Spratte, K. *Thin Solid Films* **1992**, *210/211*, 9.
(22) Spratte, K.; Chi, L. F.; Riegler, H. *Europhys. Lett.* **1994**, *25*, 211.

monolayer deposition between one phase and another, yielding patterns of parallel stripes or bands. Several chemical systems (i.e., phospholipids,[26−28] arachidic acid/cadmium arachidate,[29] lipid/lipopolymer mixture,[30] metal nanoparticles,[25,31] phospholipid/polymerization initiator mixture,[32] and organic semiconductors[33,34]) have been successfully patterned by exploiting the dewetting instabilities caused by contact line interactions, suggesting the controlled manipulation of the moving front during vertical film transfer or dip coating as a versatile method for producing linear surface patterns of materials. The appropriate choice of LB transfer parameters (transfer speed, surface pressure, temperature) and monolayer composition should introduce new opportunities for generating high-density surface patterns from amphiphilic (macro-)molecules without the restrictive need for a lateral preorganization of nanostructures at the A/W interface.

It is appropriate to acknowledge that the patterns generated using the LB approach typically exhibit variability in the feature widths and spacings. Thus, while this type of patterning may not produce the level of perfection required for technological applications, as is also the case for pattern/array formation using the self-assembly of block copolymers and nanospheres,[35] it nonetheless constitutes a readily accessible, simple, and high-throughput way to generate surface templates that are sufficiently ordered for fundamental or proof-of-concept research, such as the spatially selective metallization studies described in this paper.

Fuchs et al. demonstrated the reproducible formation of periodic arrays of phospholipid stripes (∼800 nm wide) separated by empty channels (∼200 nm wide) using the wetting instabilities caused by the substrate-mediated condensation of a dipalmitoylphosphatidylcholine (DPPC) monolayer[26] (refer to ref 5 for a comprehensive review). We subsequently reported the preparation of stripe patterns using the LB transfer of a phase-separated binary mixture of phospholipids of different hydrocarbon chain lengths.[7] The stripe patterns result from the initial self-association of like lipids (hydrophobic match) at the A/W interface during monolayer compression to give condensed domains of one lipid, that are dispersed in a fluid matrix of the second lipid, followed by the self-organization and coalescence of the lipid domains at the three-phase contact line during LB deposition. The mechanism of stripe formation has been described in a previous report.[36] The mean stripe widths could be tuned from ∼300 nm down to ∼60 nm by varying the phospholipid composition and transfer pressure.[7] What distinguishes the phospholipid stripe patterns from the domain motifs of ribbons, rods, strands, fingerprints, ripples, wires, or spaghetti[11,14,15,37,38] more typically observed in Langmuir monolayers is their highly parallel and undeviating nature. Applications of the phospholipid stripes to the selective adsorption of proteins,[39] fabrication of patterned bilayer membranes,[40] enzymatic lithography,[41] masked deposition of functionalized silanes onto silicon,[42] wet chemical etching of silicon,[4] site-specific adsorption of Au_{55} clusters from organic solvent,[26] micropatterning of cyanoacrylates using the fuming method,[43] and spatially selective deposition of silver vapor,[5] demonstrate that the patterns are sufficiently robust to be used as templates.

Scheme 1. Structures of the Phospholipids and Their Disulfide Analogues

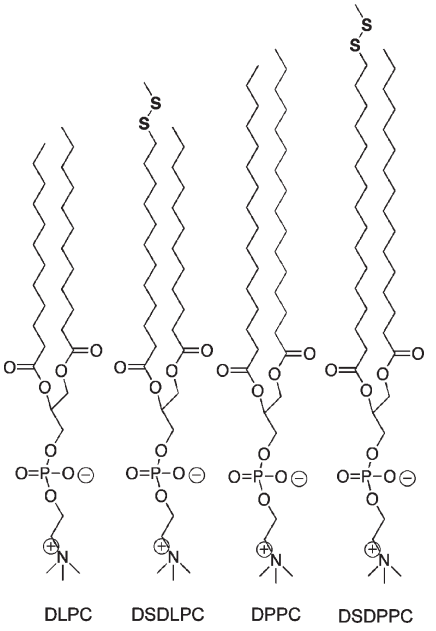

The generation of chemically differentiated patterns would expand the templating possibilities of the mixed phospholipid monolayers. The challenge lies in using a functionalized lipid that will let the mixed monolayer transfer to surfaces in stripes.[32] The original patterns were produced with the condensed-phase-forming DPPC and fluid-phase-forming dilauroylphosphatidylcholine (DLPC).[36] In this article, we investigate the monolayer film transfer of mixtures of DPPC and DLPC and their ω-methyldisulfide-terminated analogues, DSDPPC and DSDLPC (Scheme 1). Since the functionalization is limited to one of the chain ends, we expected that the phase properties and stripe-pattern-forming behavior of DSDPPC and DSDLPC would be similar to those of DPPC and DLPC.[44] We chose a methyldisulfide tag, because it is well-known that alkyldisulfides yield well-defined self-assembled monolayers (SAMs) on the surface of coinage metals by formation of a largely covalent metal−thiolate bond.[45,46] The alkyl-tail-exposed disulfides of the solid-supported DSDPPC/DLPC or

(23) Spratte, K.; Riegler, H. *Langmuir* **1994**, *10*, 3161.
(24) Raudino, A.; Pignataro, B. *J. Phys. Chem. B* **2007**, *111*, 9189.
(25) Huang, J.; Kim, F.; Tao, A. R.; Connor, S.; Yang, P. *Nat. Mater.* **2005**, *4*, 896.
(26) Gleiche, M.; Chi, L. F.; Fuchs, H. *Nature* **2000**, *403*, 173.
(27) Pignataro, B.; Sardone, L.; Marletta, G.; C, M. S. E. *Mater. Sci. Eng., C* **2002**, *22*, 177.
(28) Chen, X.; Lu, N.; Zhang, H.; Hirtz, M.; Wu, L.; Fuchs, H.; Chi, L. *J. Phys. Chem. B* **2006**, *110*, 8039.
(29) Mahnke, J.; Vollhardt, D.; Stöckelhuber, K. W.; Meine, K.; Schulze, H. J. *Langmuir* **1999**, *15*, 8220.
(30) Purrucker, O.; Förtig, A.; Lüdtke, K.; Jordan, R.; Tanaka, M. *J. Am. Chem. Soc.* **2005**, *127*, 1258.
(31) Huang, J.; Tao, A. R.; Connor, S.; He, R.; Yang, P. *Nano Lett.* **2006**, *6*, 524.
(32) Brinks, M. K.; Hirtz, M.; Chi, L.; Fuchs, H.; Studer, A. *Angew. Chem., Int. Ed.* **2007**, *46*, 5231.
(33) Li, L.; Gao, P.; Schuermann, K. C.; Ostendorp, S.; Wang, W.; Du, C.; Lei, Y.; Fuchs, H.; Cola, L. D.; Müllen, K.; Chi, L. *J. Am. Chem. Soc.* **2010**, *132*, 8807.
(34) Liu, N.; Zhou, Y.; Wang, L.; Peng, J.; Wang, J.; Pei, J.; Cao, Y. *Langmuir* **2009**, *25*, 665.
(35) Xia, Y.; Rogers, J. A.; Paul, K. E.; Whitesides, G. M. *Chem. Rev.* **1999**, *99*, 1823.
(36) Moraille, P.; Badia, A. *Langmuir* **2002**, *18*, 4414.
(37) Qaqish, S. E.; Paige, M. F. *Langmuir* **2008**, *24*, 6146.
(38) Kim, Y.; Pyun, J.; Fréchet, J. M. J.; Hawker, C. J.; Frank, C. W. *Langmuir* **2005**, *21*, 10444.
(39) Moraille, P.; Badia, A. *Angew. Chem., Int. Ed.* **2002**, *41*, 4303.
(40) Moraille, P.; Badia, A. *Langmuir* **2003**, *19*, 8041.
(41) Moraille, P.; Badia, A. *J. Am. Chem. Soc.* **2005**, *127*, 6546.
(42) Lu, N.; Gleiche, M.; Zheng, J.; Lenhert, S.; Xu, B.; Chi, L.; Fuchs, H. *Adv. Mater.* **2002**, *14*, 1812.
(43) Erickson, E. S.; Livanec, P. W.; Frisz, J. F.; Dunn, R. C. *Langmuir* **2009**, *25*, 5098.
(44) Ihalainen, P.; Peltonen, J. *Langmuir* **2002**, *18*, 4953.
(45) Nuzzo, R. G.; Zegarski, B. R.; Dubois, L. H. *J. Am. Chem. Soc.* **1987**, *109*, 733.
(46) Laibinis, P. E.; Whitesides, G. M.; Allara, D. L.; Tao, Y. T.; Parikh, A. N.; Nuzzo, R. G. *J. Am. Chem. Soc.* **1991**, *113*, 7152.

DPPC/DSDLPC monolayers introduce the possibility for the spatially selective modification of the surface with metal and the construction of regular arrays of substrate-bound metallic wires or slits that are suited for studies of the relation between the width and spacing of the nanostructures and their surface plasmon properties,[47−49] electrical conductivity,[50,51] or diffractive optics response.[52,53]

We describe the fabrication of an expansive array of organosulfur-modified phospholipid stripes on solid substrates by the LB technique and investigate the physical vapor deposition (PVD) of Au, Ag, and Cu on the chemically structured patterns. PVD was chosen because it is simple to execute, compatible with the thermal stability of phospholipid monolayers, and to date, most investigations of metal−organic thin film interactions and organic electronic device properties have employed this technology.[54] Gold and silver were chosen because of their extensive use as substrates for surface plasmon resonance spectroscopy.[55] Copper is of interest because it is employed as an interconnect material in the semiconductor industry.[56] We show, using X-ray photoelectron spectroscopy (XPS) and field emission gun scanning electron microscopy (FEGSEM), that the metal atoms react with the surface-bound disulfide groups to form a metal−thiolate species. Atomic force microscopy (AFM) measurements and cold detergent extraction of the uncoated phospholipid areas provide evidence for a preferential accumulation of metal on the reactive disulfide-functionalized regions of the patterns at submonolayer coverages of metal deposit.

Experimental Section

Materials. L-α-DPPC and L-α-DLPC were obtained as powders from Avanti Polar Lipids, Inc. (Alabaster, AL) and used without further purification (chemical purity >99%). Triton X-100 (Ultrapure) was purchased from Sigma-Aldrich Chemical Co. (St. Louis, MO). Gold granules (99.99%) were from Plasmaterial, Inc. (Livermore, CA). Silver granules (99.99%) were purchased from Kitco Metals Inc. (Montreal, QC), and copper wire was obtained from Sigma-Aldrich (99.9%). Ruby muscovite mica (ASTM grade 2) was from B&M Mica Co., Inc. (Flushing, NY) and cleaved before use. Prime-grade silicon (Si/SiO_x) wafers of type N with a resistivity of 1000−10 000 Ω−cm, thickness 500−550 μm, and particles of <10 @ 0.3 μm were purchased from WaferNet Inc. (San Jose, CA). Each Si/SiO_x substrate was first sonicated sequentially for 5 min in the following solvents: chloroform spectrograde, acetone spectrograde, and ethanol 100%. It was dried with N_2 and exposed to a piranha etch solution (3:1 concentrated sulfuric acid/30% hydrogen peroxide) for 10 min. The substrate was then dipped three times in high-purity water and kept in ethanol until use (no more than 5 h). The high-purity water (18.2 MΩ cm) used for all experiments was prepared by passing water purified by reverse osmosis through a Milli-Q Gradient System (Millipore, Bedford, MA). Its surface tension was measured to be 72.1 mN m^{-1} at 22 °C.

1-Palmitoyl-2-(16-(*S*-methyldithio)hexadecanoyl)-*sn*-glycero-3-phosphocholine (DSDPPC) was synthesized with some modifications to the procedure described by Ihalainen et al.[44] Briefly, 16-mercaptohexadecanoic acid was obtained from the ring-opening of 16-hexadecanolide (Sigma-Aldrich) to 16-hydroxyhexadecanoic acid, followed by bromination and substitution for a thiol group. 16-Mercaptohexadecanoic acid was then reacted with 1-palmitoyl-2-hydroxy-*sn*-glycero-3-phosphocholine (Avanti Polar Lipids). The synthesis of 1-lauroyl-2-(12-(*S*-methyldithio)-dodecanoyl)-*sn*-glycero-3-phosphocholine (DSDLPC) was performed in the same manner starting with cyclohexadecanone (Sigma-Aldrich) to produce 12-mercaptododecanoic acid which was then reacted with 1-lauroyl-2-hydroxy-*sn*-glycero-3-phosphocholine (Avanti Polar Lipids). Both DSDPPC and DSDLPC were characterized by ^1H NMR spectroscopy and mass spectrometry.

Langmuir−Blodgett Film Deposition. Two different troughs from KSV Instruments Ltd. (Helsinki, Finland) were used interchangeably: KSV 3000 standard trough (surface area of 768 cm^2) equipped with an Isotemp 1006D circulation bath (Fisher Scientific) and a KSV 2000 System 3 mini-alternate multilayer trough (surface area of 287 cm^2) connected to a Julabo model F12-MC circulation bath. Both troughs were equipped with a Pt Wilhelmy plate sensing device (KSV Instruments, Helsinki, Finland). The subphase temperature was maintained at 20 °C (±0.5 °C).

Solutions of DPPC, DLPC, DSDPPC, DSDLPC, DPPC/DLPC, DSDPPC/DLPC, and DPPC/DSDLPC were prepared using spectrograde chloroform to give a total phospholipid concentration of 1 mM. Monolayers were formed by spreading 100 μL of the appropriate solution on the water surface of the standard LB trough and 35 μL was spread in the mini-alternate LB trough. The solvent was allowed to evaporate for 15 min. The phospholipid molecules were symmetrically compressed at a rate of 1 $Å^2$ $molecule^{-1}$ min^{-1} up to the target deposition pressure. After a barrier stabilization time of about 20 min, the monolayer films were deposited onto mica at a constant surface pressure. The substrate was pulled vertically upward through the A/W interface at a rate of 1 or 5 mm min^{-1}. Film transfer ratios of 1.0−1.2 were obtained.

Metal Vapor Deposition by Resistive Thermal Evaporation. Nominal metal thicknesses ranging from 0.15 to 1.0 nm were deposited at a rate of 0.1 Å s^{-1} onto the phospholipid-patterned mica or silicon using a VE-90 thermal evaporator equipped with a quartz crystal deposition monitor (Thermionics Vacuum Products, Port Townsend, WA). The metal evaporation process was initiated once a base pressure of $< 5.5 \times 10^{-7}$ Torr was attained and there was no cooling or heating of the substrates. The evaporation time ranged from 8 to 50 s, depending on the thickness of metal evaporated, and the maximal temperature near the rotating sample stage was 70 °C (evaporation source to sample distance of 38 cm). The deposited metal thicknesses reported in this article are the mass thicknesses indicated by the calibrated quartz crystal monitor.

Detergent Extraction. The solid-supported monolayer film temperature was lowered to 4 °C (measured with a thermocouple) by leaving the sample in the freezer for 10 min. The sample was then removed from the freezer, and 1 mL of an aqueous 1% v/v Triton X-100 solution (cooled to 4 °C before use) was used to cover a 1 cm^2 area. After 30 s, the Triton X-100 drop was removed and the treated area was rinsed with water and blown dry with nitrogen. The sample was then imaged in air by AFM.

AFM Imaging. Two scanning probe microscopes from Veeco Metrology Inc. (Santa Barbara, CA) were used interchangeably to image the samples under ambient conditions: a Dimension 3100 scanning probe microscope and an EnviroScope atomic force microscope. Both microscopes were equipped with a Nanoscope IIIa controller and a Quadrex Extender module. Height and phase contrast images were simultaneously acquired in intermittent-contact ("tapping") mode using a damping of 70−85% of the free oscillation amplitude of silicon probes (type PPP-NCH, Nanosensors) of nominal spring constant of 42 N m^{-1}, resonance frequency 330 kHz, and tip radius of curvature of <10 nm. Images were captured at scan rates 1−1.5 Hz and a resolution of 512 × 512 pixels.

(47) Jara, A.; Arias, R. E.; Mills, D. L. *Phys. Rev. B* **2010**, *81*, 085422.
(48) Stewart, M. E.; Anderton, C. R.; Thompson, L. B.; Maria, J.; Gray, S. K.; Rogers, J. A.; Nuzzo, R. G. *Chem. Rev.* **2008**, *108*, 494.
(49) Lee, K.-L.; Wang, W.-S.; Wei, P.-K. *Plasmonics* **2008**, *3*, 119.
(50) Chai, J.; Wang, D.; Fan, X.; Buriak, J. M. *Nat. Nanotechnol.* **2007**, *2*, 500.
(51) Lopes, W. A.; Jaeger, H. M. *Nature* **2001**, *414*, 735.
(52) Bailey, R. C.; Nam, J.-M.; Mirkin, C. A.; Hupp, J. T. *J. Am. Chem. Soc.* **2003**, *125*, 13541.
(53) Goh, J. B.; Loo, R. W.; Goh, M. C. *Sens. Actuators, B* **2005**, *106*, 243.
(54) Walker, A. V. *Langmuir* Article ASAP, DOI: 10.1021/la903937u.
(55) Zynio, S. A.; Samoylov, A. V.; Surovtseva, E. R.; Mirsky, V. M.; Shirshov, Y. M. *Sensors* **2002**, *2*, 62.
(56) Monteiro, O. R. *J. Vac. Sci. Technol., B* **1999**, *17*, 1094.

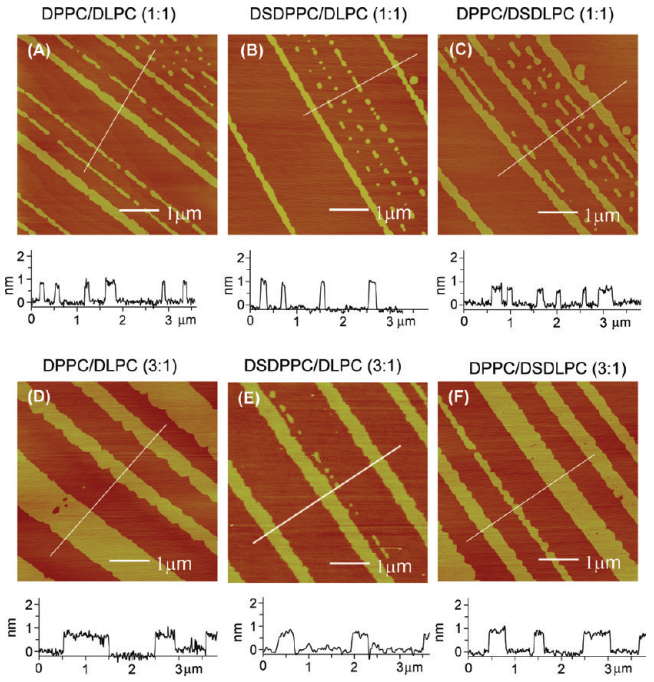

Figure 1. AFM images and line cross sections of mica-supported films (except (E) supported on Si/SiO_x). Mixtures 1:1 (mol/mol) of (A) DPPC/DLPC, (B) DSDPPC/DLPC, and (C) DPPC/DSDLPC. Mixtures 3:1 (mol/mol) of (D) DPPC/DLPC, (E) DSDPPC/DLPC, and (F) DPPC/DSDLPC.

X-ray Photoelectron Spectroscopy (XPS). The X-ray photoelectron spectra were obtained using an ESCALAB 3 MKII spectrometer (VG Scientific) equipped with a Mg Kα source. A takeoff angle of 70° from the surface was used. The survey spectra were recorded with a power of 206 W (12 kV, 18 mA), a 100 eV pass energy, and steps of 1.0 eV. The high-resolution scans were acquired with a pass energy of 20 eV and steps of 0.05 eV. The size of the area analyzed was 2 mm×3 mm. The spectra were referenced to C1s at 286.6 eV. A Shirley background was applied to the high-resolution spectra and the peaks were fit using a symmetric Voigt function with a variable Lorenz-Gauss ratio. The Au 4f spectra were fit with a doublet with the same full width at half-maximum (fwhm) of 1.33, a spin−orbit splitting of 3.67 eV, and a height ratio (Au $4f_{7/2}$/Au $4f_{5/2}$) of 5:4. The S2p spectra were fit with a doublet with the same fwhm of 1.45, a spin−orbit splitting of 1.18 eV, and a height ratio (S $2p_{3/2}$/S $2p_{1/2}$) of 2:1.

Field Emission Gun Scanning Electron Microscopy (FEGSEM). Samples were imaged using a Hitachi S-4700 instrument. Secondary electron images were acquired at 2 kV, 10 μA, and 4.6−5.0 mm working distance.

Spectroscopic Ellipsometry. A film thickness of 3.25 ± 0.07 nm was obtained for pure condensed DSDPPC monolayers deposited on silicon substrates at $\pi = 32$ mN m^{-1}. All measurements were performed in air at an incident angle of 75° and a wavelength range of 370−1000 nm on a multiwavelength ellipsometer equipped with a QTH lamp and rotating compensator (model M-2000 V, J. A. Woollam Co, Inc., Lincoln, NE), as previously described.[17] The phospholipid monolayers were modeled as Cauchy (transparent) layers using the dispersion equation $n(\lambda/\mu m) = A + B/\lambda^2 + C/\lambda^4$, where $n(\lambda)$ is the wavelength-dependent refractive index and A, B, and C are the Cauchy parameters. The data was fit using values for the Cauchy parameters of $A = 1.44$, $B = 0.0045$, and $C = 0$. At 532.3 nm, $n = 1.456$ and $k = 0$.

Results and Discussion

Surface Morphology of LB Monolayers. Langmuir monolayers formed from 3:1 or 1:1 (mol/mol) binary mixtures of DPPC/DLPC, DPPC/DSDLPC, and DSDPPC/DLPC were transferred onto mica or Si/SiO_x at surface pressures (π) greater than or approximately equaling the composition-dependent, liquid-expanded-to-condensed (LE-to-C) transition pressures of the phospholipid mixtures, as described in our previous work.[7,57,58] Typical AFM images of the solid-supported films are shown in Figure 1. Patterns consisting of thicker parallel stripes (DPPC- or DSDPPC-enriched phase) surrounded by a thinner matrix (DLPC- or DSDLPC-enriched phase) are observed for all three mixtures. The condensed-phase stripe domains protrude above the LE or fluid background matrix by ∼0.9 nm for DPPC/DLPC and DSDPPC/DLPC and ∼0.7 nm for DPPC/DSDLPC. A characteristic feature of all the patterns is that wider continuous stripes are periodically interspersed among a more closely spaced series of narrower broken stripes. Mixed monolayers of the 3:1 composition, containing more of the condensed-phase forming DPPC or DSDPPC versus the fluid-phase forming DLPC or DSDLPC, exhibit stripes that are approximately twice as wide as those of monolayers of equimolar composition. The mean stripe widths obtained from an analysis of the AFM images are given in Table 1. The center-to-center stripe spacing ranges from ∼400 nm to ∼3 μm. The stripe widths and spacings depend on the molar ratio of condensed phase to fluid phase phospholipid, film transfer pressure, and film transfer speed. Only a limited set of conditions was explored here, such that the narrowest DSDPPC stripe width of 145 nm reported in Table 1 should not be viewed as the lower limit of feature size that can be generated. We previously obtained 60-nm-wide stripes from the LB transfer of a 0.15:0.85 DPPC/DLPC monolayer at high surface pressure.[7] Micrometer-sized, condensed circular domains coexist with the stripes under the Langmuir monolayer formation and deposition conditions used in this work, as revealed by the larger field-of-view accessible in FEGSEM. In the 3:1 DSDPPC/DLPC monolayers, for example, there are typically 9 to 10 circular domains of ∼10 to ∼20 μm diameter in a 0.023 mm^2 area, and the stripe motifs extend over areas ≳30 × 30 μm^2 DLPC (Supporting Information Figure S1A), while fewer (or no) domains are observed in the same size area for the 3:1 DPPC/DLPC (Supporting Information Figure S1B). Efforts are currently underway to improve the regularity of the stripe motifs (i.e., uniformity of stripe widths and spacings) by varying the Langmuir monolayer formation and LB film

Table 1. Average Widths of the Stripes in the Mixed Monolayer Patterns

monolayer	$\pi_{\text{film transfer}}$/mN m^{-1}	width of continuous stripes/nm
	DPPC/DLPC	
3:1 [a]	8	290 ± 140 (n = 119)
1:1 [b]	16	174 ± 73 (n = 92)
	DPPC/DSDLPC	
3:1 [a]	12	480 ± 230 (n = 20)
1:1 [b]	18	170 ± 95 (n = 32)
	DSDPPC/DLPC	
3:1 [a]	12	300 ± 160 (n = 181)
1:1 [b]	18	145 ± 60 (n = 73)

[a] Substrate withdrawal speed from A/W interface = 1 mm min^{-1}. [b] Substrate withdrawal speed from A/W interface = 5 mm min^{-1}.

(57) Sanchez, J.; Badia, A. *Thin Solid Films* **2003**, *440*, 223.
(58) A detailed comparison of the monolayer film properties of the methyldithio-modified phospholipids with those of the unmodified lipids will be reported elsewhere.

deposition conditions and through the use of lineactants such as cholesterol.[59]

The solid-supported monolayers generated herein have their ω-methyldithio (-SS-) groups exposed at the surface and phosphocholine headgroups adsorbed to the mica or Si/SiO_x. Assuming that DSDPPC and DSDLPC occupy roughly the same molecular areas in the stripes and background matrix of the phase-separated mixed monolayers as they occupy in the single component systems at a given film transfer pressure, we estimate 1.5 to 1.8 -SS- groups per nm^2 for the stripe domains of DSDPPC/DLPC and 0.96 to 1.1 -SS- groups per nm^2 for the background matrix of DPPC/DSDLPC.[60] These disulfide surface coverages should be taken as the theoretical or maximum values, because previous work with DPPC/DLPC revealed a positive deviation between the experimentally determined mean molecular areas of binary mixtures and those calculated from the areas of the pure DPPC and DLPC using the additivity rule.[57]

Physical Vapor Deposition of Metals. Resistive thermal evaporation was used to deposit different thicknesses of gold, silver, and copper onto the phospholipid monolayers. The atomic radii and corresponding coverages of the different metals are given in Table 2. The nominal layer thicknesses of vapor-deposited metal reported in this article are the average mass thicknesses indicated by a calibrated quartz crystal microbalance during metal evaporation. Gold-coated films were analyzed by XPS to confirm the presence of metal on the phospholipid surfaces and characterize the metal−disulfide interaction. FEGSEM and AFM were used to evaluate the spatial distribution of the metals on the surface of the mixed phospholipid patterns.[61]

XPS Analysis. For all of the films analyzed, only the expected elements were observed: C, N, P, S, O, Si, and Au (Supporting Information Figure S2). We do not compare herein the expected atomic concentrations with those derived from XPS or report elemental ratios, since the calculated atomic composition is sensitive to the XPS operating conditions, including the takeoff angle and the elemental distribution perpendicular to the surface, and variable angle measurements were not performed.[62] The presence of a doublet (Au 4f) between 84 and 88 eV and peaks at ∼335 and ∼353 eV (Au 4d) in the XPS survey scans following thermal evaporation confirmed the presence of Au on the mixed monolayer surfaces (Supporting Information Figure S2). High-resolution XPS scans were run on single-component monolayers in the condensed state ($\pi_{\text{film transfer}} = 20\ \text{mN m}^{-1}$) to increase the coverage of the ω-methyldithio groups at the DSDPPC monolayer surface and the intensity of the sulfur signal. The Au 4f and S 2p spectra lines were measured, as these are the core levels reported in studies of SAMs of alkanethiolates on planar gold substrates (RS-Au), alkanethiolate-capped Au nanoparticles, and polymeric Au(I)-thiolate complexes.[46,62−66] Typical S $2p_{3/2}$ binding energies (BEs) for nonbound *n*-alkylthiols (RSH) and *n*-alkyldisulfides (RSSR) range 163−164 eV.[66] Chemisorption of these two classes of organosulfur compounds to gold substrates yields indistinguishable S2p spectra, indicating that both precursors form the same species on the surface.[63] The S $2p_{3/2}$ BE shifts to 162 eV,[46,62−66] a value indicative of a covalent gold−sulfur bond with thiolate-like character (i.e., the charge per S is about $-0.2e$).[64] Although the photoelectron peak intensities of the Au $4f_{7/2}$ and $4f_{5/2}$ core levels are in some cases attenuated by the overlying SAM (long alkyl chain), their BEs remain at values expected for Au^0 after chemisorption of the thiol or disulfide.[46,62−65]

Table 2. Atomic Radii and Nominal Thicknesses of the Thermally Evaporated Metals

	gold (Au)	silver (Ag)	copper (Cu)
atomic radius	0.144 nm	0.144 nm	0.128 nm
1 monolayer (1 ML)	0.288 nm	0.288 nm	0.256 nm
nominal thickness of 0.15 nm	0.52 ML	0.52 ML	0.59 ML
nominal thickness of 0.25 nm	0.87 ML	0.87 ML	0.98 ML

Table 3. Binding Energies from High-Resolution XPS spectra of DPPC and DSDPPC with and without a 1 ML (0.30 nm) Coating of Au

	binding energy/eV (relative at %)[b]	
Si/SiO_x-supported monolayer[a] (no. of samples analyzed)	Au $4f_{7/2}$	S $2p_{3/2}$
DPPC + 1 ML Au (n = 1)	84.0	-
DSDPPC (n = 2)	-	163.0 ± 0.1
DSDPPC + 1 ML Au (n = 3)	83.9 ± 0.2	161.8 ± 0.6 (66 ± 10%) 163.4 ± 0.6 (34 ± 10%)

[a] $\pi_{\text{film transfer}} = 20\ \text{mN m}^{-1}$. [b] For multiple contributions to a given signal.

The BE values obtained from a deconvolution of the high-resolution spectra of DPPC and DSDPPC with or without a 1 ML (0.30 nm) Au coating are presented in Table 3. The Au 4f spectra were fitted using one doublet with splitting of 3.7 eV (Figure 2A,B). The Au $4f_{7/2}$ BEs of 83.9−84.0 eV correspond to Au^0. As in the case of RS-Au SAMs, there is neither a Au(I)-associated peak (BE ≈ 84.3 eV),[64] nor evidence for more than one Au state in the spectrum of the Au-coated DSDPPC. The S 2p spectrum of DSDPPC (Figure 2C) shows an asymmetric peak, which could be fitted using a doublet of area ratio of 2:1 and splitting of 1.2 eV (i.e., the spin−orbital-coupled doublet of this core level is unresolved under the acquisition conditions employed). The S $2p_{3/2}$ BE of 163.0 eV is well within the range of values reported for free thiols and disulfides. The S 2p spectrum of the Au-coated DSDPPC is shown in Figure 2D. The presence of a Au overlayer attenuates the spectral intensity. The S 2p peak can be fit reasonably well, despite the noise in the spectrum, as two doublets with area ratios of 2:1 and splittings of 1.2 eV. No peaks due to oxidized sulfur species (S 2p BE > 166 eV),[66] such as sulfoxides, sulfones, or sulfonates, were detected. The S $2p_{3/2}$ BEs are 161.8 and 163.4 eV. These values are attributable to a gold-bound thiolate species and to nonbound disulfide moieties. The dissociative addition of DSDPPC to Au can yield Au-SCH_3 (assuming a stable surface CH_3S−Au species can form)[45] and Au-SDPPC. Our XPS data (S 2p, C 1s) do not allow us to establish whether both gold−thiolates are formed or whether Au-SDPPC is the predominant species.[67,68] Future characterization work will make use of spontaneous desorption time-of-flight mass spectrometry for identification of the gold-bound surface species.[69]

The relative area contribution of the bound thiolate peak to the S $2p_{3/2}$ signal suggests that ∼66% of the sulfurs are bound to Au.[70] It is unlikely that the nonbound population (∼34%) is a CH_3SSCH_3 byproduct from a preferential reaction of -SDPPC

(59) McConnell, H. M.; Keller, D.; Gaub, H. *J. Phys. Chem.* **1986**, *90*, 1717.
(60) Values were calculated from the molecular areas occupied by the pure phospholipids at the A/W interface at a given surface pressure.
(61) We do not presently have access to a TOF-SIMS and Scanning Auger Microscope with sufficient lateral resolution (< 100 nm) to perform compositional mapping of our functionalized stripe patterns.
(62) Bain, C. D.; Troughton, E. B.; Tao, Y. T.; Evall, J.; Whitesides, G. M.; Nuzzo, R. G. *J. Am. Chem. Soc.* **1989**, *111*, 321.
(63) Bain, C. D.; Biebuyck, H. A.; Whitesides, G. M. *Langmuir* **1989**, *5*, 723.
(64) Bourg, M.-C.; Badia, A.; Lennox, R. B. *J. Phys. Chem. B* **2000**, *104*, 6562.
(65) Castner, D. G.; Hinds, K.; Grainger, D. W. *Langmuir* **1996**, *12*, 5083.
(66) NIST X-ray Photoelectron Spectroscopy Database, Reference Database 20, Version 3.5, **2003**.
(67) Heister, K.; Allara, D. L.; Bahnck, K.; Frey, S.; Zharnikov, M.; Grunze, M. *Langmuir* **1999**, *15*, 5440.

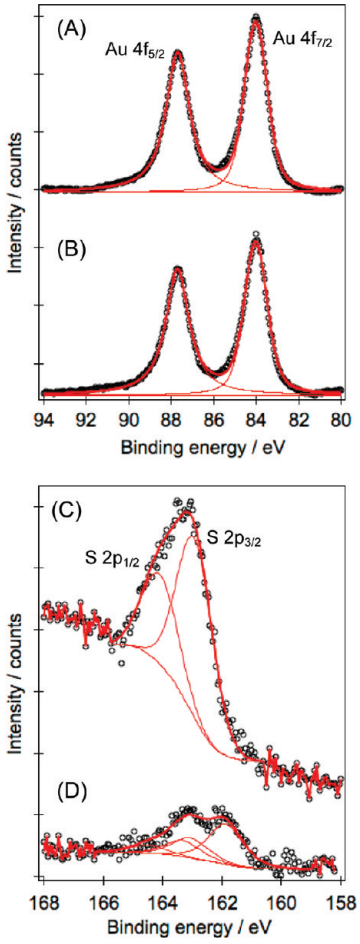

Figure 2. High-resolution XPS spectra. Au 4f doublet for (A) DPPC and (B) DSDPPC + 1 ML of Au. S 2p spectra of (C) DSDPPC and (D) DSDPPC + 1 ML of Au.

with Au, as this highly volatile compound (vapor pressure of 3.8 kPa at 20 °C),[71] if formed, should be pumped off the surface in the vacuum chambers of the metal evaporator (base pressure $\sim 10^{-7}$ Torr) and XPS instrument ($\sim 10^{-9}$ Torr). The signal at 163 eV is most likely due to nonreacted DSDPPC. The presence of free methyldithio groups cannot be ascribed to an insufficient quantity of evaporated Au (i.e., 1 ML) on the DSDPPC surface given that the Au:S ratio is ~4:1,[72] and that Au/S stoichiometries of 3:1, 2:1, and 1:1 are necessary to fulfill the range of Au (surface):S ratios reported for RS-Au SAMs on extended (planar) and finite (nanoparticle) surfaces.[64,73] The incomplete reaction may be due to the formation of Au clusters, as opposed to a continuous monatomic layer, on the DSDPPC surface (vide infra Figure 5), with only the Au atoms in direct contact with the underlying DSDPPC surface reacting with the -SS- groups. However, differences in reactivity between the solid (disulfide)/gas (Au) configuration used herein and the solid (Au)/solution (disulfide) configuration typically used for the self-assembly of RSH or RSSR on metals cannot be excluded. In summary, XPS establishes that there is reaction of the solid DSDPPC film surface with the evaporated Au atoms to form a gold−thiolate species.

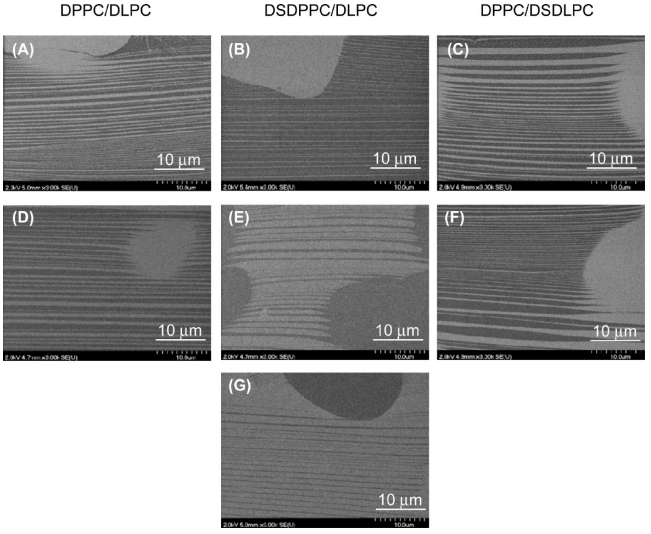

Figure 3. FEGSEM micrographs of Si/SiO_x-supported monolayers formed from 3:1 mixtures. (A) DPPC/DLPC, (B) DSDPPC/DLPC, and (C) DPPC/DSDLPC. (D) DPPC/DLPC, (E) DSDPPC/DLPC, and (F) DPPC/DSDLPC coated with 0.87 ML (0.25 nm) of Au. (G) DSDPPC/DLPC coated with 2 ML (0.60 nm) of Au.

FEGSEM Imaging. Various reports have demonstrated the secondary electron mode of FEGSEM to be extremely sensitive at low acceleration voltages to variations in surface composition and structure.[74] The contrast observed in micrographs is due to spatial variations in the surface work function and secondary electron emission between the different molecular components. Figure 3 shows FEGSEM images of Si/SiO_x-supported monolayers. The 3:1 mixtures were used for FEGSEM because the larger stripes (i.e., mean widths of 300−500 nm) are better resolved. The condensed stripe domains and LE background matrix appear as parallel bands of different contrast. The secondary electron emission intensity of the larger circular domains of condensed phospholipid was used to identify the linear regions of the image that are condensed phase stripes and those that are the fluid phase background. The light gray circular domains and stripes (high emission intensity) in the micrographs of the bare monolayers (Figure 3A−C) are attributable to the condensed phase of DPPC or DSDPPC and the surrounding dark regions (low emission intensity) are the DLPC- or DSDLPC-containing fluid matrix. This assignment is consistent with previous work in which Bitterman et al.[75] imaged chemically homogeneous phospholipid

(68) The self-assembly of asymmetric *n*-dialkyl disulfides (R_1SSR_2), where $R_1 \ll R_2$, under typical solution conditions gives large deviations from the expected 1:1 R_1S-:R_2S- surface composition. The SAMs formed consist predominantly of the longer chain R_2S-Au species, due to a surface/solution exchange mechanism which results in a almost complete substitution of the adsorbed shorter chains of the SAMs by the longer ones. On the basis of this previous work, one would expect the di-C_{16} chain phospholipid thiolate to be the predominant gold-bound species. Nevertheless, a similar thiolate exchange/substitution process may not be operative in the DSDPPC-Au system because a heterogeneous solid/gas, as opposed to solid/solution, reaction is involved here and there is no external reservoir of DSDPPC available for thiolate exchange. For this reason, the S2p spectrum may reflect contributions from both Au-SCH_3 and Au-SDPPC.

(69) Aliganga, A. K. A.; Duwez, A.-S.; Mittler, S. *Org. Electron.* **2006**, *7*, 337.

(70) 1 ML of Au was also evaporated on a DSDPPC monolayer transferred at higher surface pressure (32 mN m^{-1}). No significant difference in the extent of the surface reaction was observed: 62% bound thiolate (161.8 eV) and 38% unbound sulfur (163.3 eV).

(71) Service du répertoire toxicologique, Commission de la santé et de la sécurité du travail (CSST), Workplace Hazardous Materials Information System: http://www.reptox.csst.qc.ca/Produit.asp?no_produit=166371&nom=Dimethyl+disulfide (accessed May 19, 2010).

(72) At a film transfer pressure of 20 mN m^{-1}, DSDPPC occupies a molecular area of 0.50 ± 0.03 nm^{-2}, so that the surface concentration of -SS- groups in the monolayer is 2.0 ± 0.1 nm^{-2}. The surface coverage of Au atoms in 1 ML is 15.4 nm^{-2}, yielding a mean Au:S ratio of 3.8:1.

(73) Luedtke, W. D.; Landman, U. *J. Phys. Chem.* **1996**, *100*, 13323.

(74) Srinivasan, C.; Mullen, T. J.; Hohman, J. N.; Anderson, M. E.; Dameron, A. A.; Andrews, A. M.; Dickey, E. C.; Horn, M. W.; Weiss, P. S. *ACS Nano* **2007**, *1*, 191.

(75) Bittermann, A. G.; Jacobi, S.; Chi, L. F.; Fuchs, H.; Reichelt, R. *Langmuir* **2001**, *17*, 1872.

monolayers with domains of varying molecular packing density and found that regions with higher packing density (condensed phase) emit more secondary electrons and exhibit a higher intensity in FEGSEM images than areas of lower packing density (LE phase). That the same contrast is observed for the chemically homogeneous DPPC/DLPC monolayer and the chemically heterogeneous DSDPPC/DLPC and DPPC/DSDLPC films indicates that the secondary electron emission intensity is dominated by the molecular packing density under the given operating conditions.

Figure 3D−F are the micrographs after the evaporation of 0.87 ML (0.25 nm) of Au. An inversion of contrast is observed in the case of DSDPPC/DLPC (Figure 3E vs B), which persists after the evaporation of 2 ML (0.60 nm) of Au (Figure 3G). The DSDPPC-enriched circular domains and stripes are darker (lower intensity) than the surrounding DLPC-containing matrix. No such contrast inversion occurs in the chemically homogeneous DPPC/DLPC monolayer (Figure 3D vs A), which should be uniformly covered with gold.[76] The gold coating attenuates the secondary electron emission from the DSDPPC-enriched domains, rendering it weaker than that of the DLPC background. Two different effects can cause the observed signal attenuation: (i) the preferential location of the evaporated gold in the reactive DSDPPC regions, with or without formation of a Au-thiolate bond between some of the Au atoms and the methyldithio end groups, or (ii) formation of Au-thiolate species on the DSDPPC domains of a fully gold-covered surface. We will return to the likely origin of the FEGSEM contrast later on in the discussion. No attenuation of the DSDLPC background matrix with respect to the DPPC domains is evident in the complementary DPPC/DSDLPC system because the secondary emission intensity is already low in the absence of deposited gold (Figure 3F vs C).

AFM Imaging. To rationalize the differences in image contrast observed in FEGSEM for the different gold-coated monolayer surfaces, the stripe-to-background matrix step height (Δh) and film morphology were analyzed by tapping-mode AFM. Figure 4 shows topography images of 1:1 mixed monolayer films after deposition of 0.5 ML (0.15 nm) of Au. The stripe-to-background height difference ($\Delta h \approx 0.9$ nm) remains the same for the nonfunctionalized DPPC/DLPC pattern (Figure 4A), consistent with a homogeneous distribution of Au across the surface. In the case of the DSDPPC/DLPC template, where the -SS- moieties are located in the stripe domains (Figure 4B), Δh increases by 0.3 nm, suggesting the preferential (but not necessarily exclusive) accumulation of gold onto the stripes. When the -SS- groups are localized in the background matrix phase (DPPC/DSDLPC), there is no obvious change in step height (within the standard deviation) after the evaporation of 0.5 ML of Au (Figure 4C). However, cold detergent extraction of the unprotected lipid phase reveals that the Au is concentrated at the DSDLPC matrix (vide infra Figure 6). Because of the more disordered fluid nature of the background phase, the selectivity of the Au deposition onto DPPC/DSDLPC could not be evaluated through AFM measurements of the step height.

The deposition of silver and copper onto the 1:1 DSDPPC/DLPC pattern was also investigated (Table 4). Both metals behaved like gold at submonolayer coverages, an increase in the step height is observed when 0.5 to 0.6 ML of metal is thermally evaporated onto the DSDPPC/DLPC pattern. In all cases, the increase in Δh of 0.3−0.5 nm is greater than the nominal thickness of metal evaporated (i.e., 0.15 nm). Cluster-like features are

(76) There is no evidence that the Au atoms penetrate through the more liquid-like DLPC phase and accumulate on top of the solid-like DPPC domains.

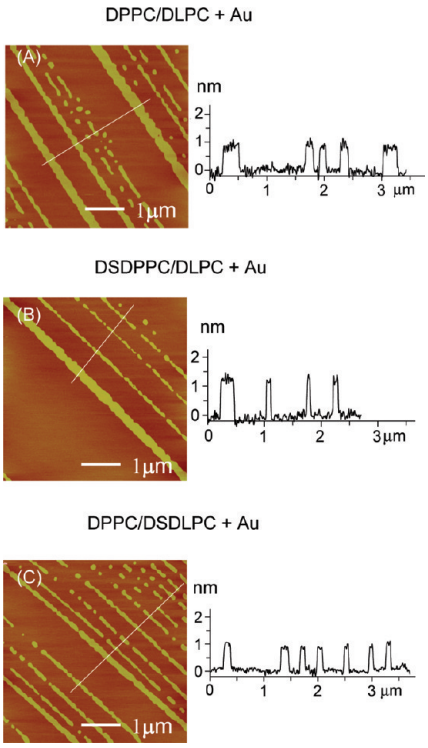

Figure 4. AFM images and line sections of 1:1 mixtures of (A) DPPC/DLPC, (B) DSDPPC/DLPC, and (C) DPPC/DSDLPC coated with 0.52 ML (0.15 nm) of Au.

Table 4. AFM-Measured Step Heights on DSDPPC/DLPC (1:1) Monolayers before and after Metal Evaporation

	step height/nm		
average layer thickness of evaporated metal[a]/nm	Au	Ag	Cu
0	0.90 ± 0.07	0.90 ± 0.07	0.90 ± 0.07
0.15	1.22 ± 0.10	1.36 ± 0.10	1.28 ± 0.08
0.25	1.26 ± 0.10	1.16 ± 0.11	0.96 ± 0.09

[a] As indicated by a quartz crystal microbalance during thermal evaporation.

clearly visible on the DSDPPC stripes in high-resolution topography, and in some cases phase, images of metal-coated DSDPPC/DLPC films (Figure 5E,G,I). No such features are discernible on the metal-coated DPPC stripes (Figure 5C). These clusters presumably form via reaction of the metal vapor with the -SS- moieties, followed by metal−metal aggregation. Due to the surface roughness of the underlying DSDPPC stripes and AFM tip convolution effects (tip radius of curvature $\lesssim$10 nm), it was not possible to obtain accurate cluster sizes.

The phase imaging mode of tapping-mode AFM was used to further characterize the metal-coated patterns. Phase imaging goes beyond topography to detect spatial variations in mechanical and chemical properties. The phase images of the bare DPPC/DLPC[7] and DSDPPC/DLPC monolayers (Figure 5B) exhibit a positive shift of ~2.5° over the stripes compared to the background phase. A positive phase shift indicates that the stripes are stiffer than the background, consistent with the solid-like nature of DPPC and DSDPPC (stripes) compared to the fluid-like DLPC (background matrix).[7] The unmodified DPPC stripes of the DPPC/DLPC monolayer, for which the topography images indicate a uniform distribution of metal across the surface, retain their positive shift (2.5°) after metal evaporation (Figure 5D). By

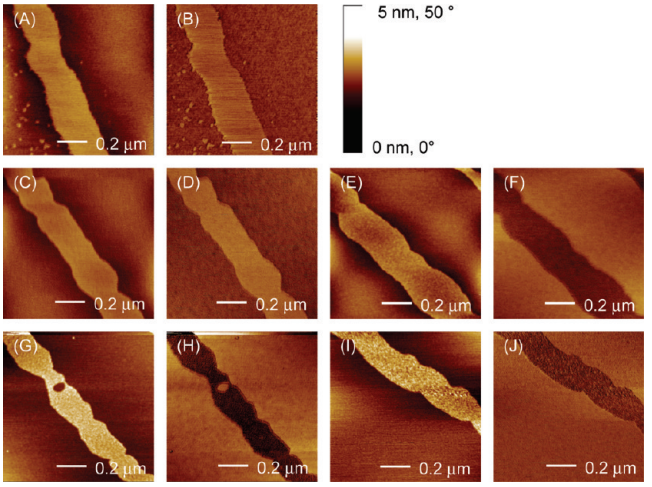

Figure 5. AFM images of (1:1) mixed monolayers. DSDPPC/DLPC (A) topography and (B) phase; DPPC/DLPC + 0.52 ML (0.15 nm) Au (C) topography and (D) phase; DSDPPC/DLPC + 0.52 ML of Au (E) topography and (F) phase; DSDPPC/DLPC + 0.87 ML (0.25 nm) Ag (G) topography and (H) phase; DSDPPC/DLPC + 0.52 ML (0.13 nm) Cu (I) topography and (J) phase.

contrast, images of DSDPPC/DLPC, onto which 0.5−0.9 ML of Au or Ag or 0.6 ML of Cu are evaporated, consistently show a reversed phase contrast over the stripes. A negative phase shift ranging 2−7° is observed over the DSDPPC stripes versus the background DLPC phase (Figure 5F,H,J), suggesting that their mechanical and/or chemical properties have been selectively altered by the deposition of an ultrathin metal layer.

Cold Detergent Extraction. Evidence for the spatial localization of the metal deposits was sought using cold detergent (Triton X-100) extraction. Cold nonionic detergent is commonly used in biology to solubilize and remove lipids from cell membranes.[40,77] We reasoned that the presence of metal deposit should prevent the underlying phospholipid from being removed from the mica surface by the detergent. The bare (uncoated) monolayer patterns are destroyed by the detergent treatment. The DPPC/DLPC monolayer covered with 0.5 ML of Au is unaffected by treatment with cold Triton X-100. The stripe-to-background step height remains the same after detergent treatment (Figure 6A vs Figure 4A), indicating that the evenly distributed Au layer acts as a protective barrier against the detergent. Figure 6B shows a DSDPPC/DLPC monolayer covered with 0.5 ML of Au following cold detergent extraction. The Δh increases from 1.2 ± 0.1 nm (before, Figure 4B) to 3.6 ± 0.5 nm (after, Figure 6B), a value consistent with the thickness of a bare DSDPPC monolayer, 3.25 nm (measured by ellipsometry), plus the thickness of Au on top of the stripes, 0.3 nm (i.e., Δh increase following Au evaporation). This increase in step height, from 1.2 to 3.6 nm, is therefore attributable to the removal, by the detergent, of the unprotected DLPC phase from the laterally differentiated monolayer film, leaving the gold-covered DSDPPC stripes untouched. Similarly, when the gold-covered DPPC/DSDLPC monolayer is treated with Triton X-100, the unprotected DPPC is removed from the pattern, resulting in linear grooves and circular holes of ~4 nm depth, as shown in Figure 6C.

We proceeded to use the Δh measured after cold detergent extraction of DSDPPC/DLPC monolayers coated with increasing Au thicknesses as an indicator of the extractable (i.e., non-

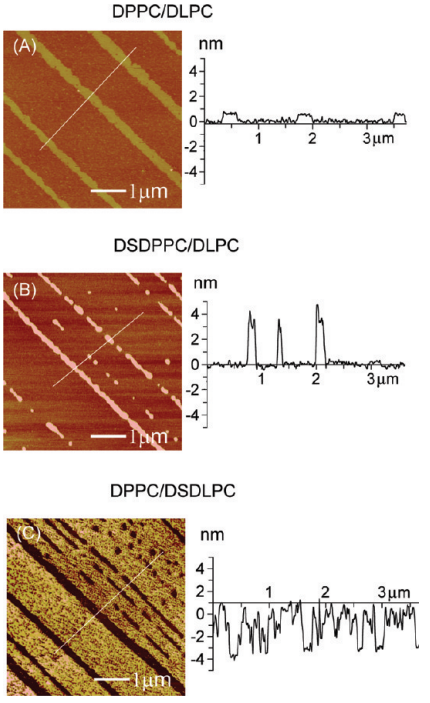

Figure 6. AFM images and line cross sections of 1:1 mixtures of (A) DPPC/DLPC, (B) DSDPPC/DLPC, and (C) DPPC/DSDLPC coated with 0.52 ML (0.15 nm) of Au followed by Triton X-100 extraction.

coated or poorly coated) DLPC phase (Supporting Information Figure S3). The step height decreased from ~3.6 nm for 0.5 ML Au to ~2.2 nm for 1.0 ML Au. For 2.1 ML of evaporated Au, the step height of ~1.5 nm is close to the value of ~1.2 nm measured before detergent treatment. This trend points to an increasing coverage of Au on the DLPC matrix. There is clearly no preferential accumulation of Au on the stripes at coverages of vapor-deposited metal greater than or equaling 1 ML.

Selectivity of the Metal Deposition versus Evaporated Metal Thickness. Having established some preference of the metal for the ω-methyldithio-containing regions at sub-ML coverages, we proceeded to determine the quantity of metal that could be thermally evaporated before the observed selectivity is lost. Plots of Δh versus the nominal thickness of Au evaporated onto 1:1 DPPC/DLPC and DSDPPC/DLPC patterns are shown in Figure 7. As expected for the uniform adsorption of metal across the unmodified DPPC/DLPC surface, Δh is constant at 0.9 ± 0.1 nm for evaporated Au thicknesses from 0 to 2.1 ML (0.60 nm). For DSDPPC/DLPC, Δh increases by ~0.29 nm on going from 0 to 0.28 ML (0.08 nm) of Au and remains at ~0.3 nm up to 2.1 ML (0.60 nm) of Au. The data presented in Figure 7 imply that the selectivity of the Au for the DSDPPC stripes is already lost above ~0.28 ML, the smallest quantity of Au that can be reliably deposited using our metal evaporator. This value is of similar magnitude to the average Au thickness (0.1 ML or 0.03 nm) expected to give a 1:1 Au:S ratio for the equimolar DSDPPC/DLPC mixture (i.e., assuming 1.8 -SS-/nm^2 and 42% area coverage by the stripes). Similar results were obtained for Ag and Cu (Table 4), although these metals were not studied in as much detail as Au. The DSDPPC/DLPC step height decreases as the nominal evaporated metal thickness increases from 0.15 to 0.25 nm, indicating a clear loss of preference of these metals for the DSDPPC.

The nonselective nature of the metal deposition demonstrated by the cold detergent extraction experiment and AFM measurements of the step height at evaporated Au thicknesses of 1 and

(77) Rinia, H. A.; Snel, M. M. E.; van der Eerden, J. P. J. M.; de Kruijff, B. *FEBS Lett*. **2001**, *501*, 92.

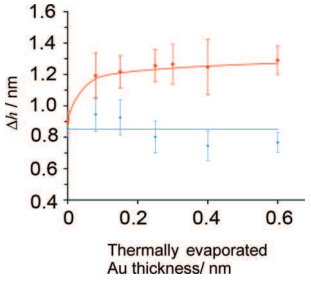

Figure 7. Step height (Δh) vs the nominal thickness of Au evaporated onto 1:1 DPPC/DLPC (blue) and DSDPPC/DLPC (red) patterns. Line and curve serve as guides to the eye.

2 ML suggest that the contrasts observed for the metal-coated DSDPPC/DLPC in FEGSEM (Figure 3E,G) and AFM phase imaging (Figure 5) originate from the formation of a metal−thiolate species on the reactive DSDPPC domains rather than reflecting the absence of metal in the DLPC background.

The very limited selectivity in metal vapor deposition observed with the chemically differentiated phospholipid-based pattern is in marked contrast with the highly selective aggregation of metals reported for ultrathin diblock copolymer films based on the preferential wetting of one block, polystyrene (PS), versus another, poly(methylmethacrylate) (PMMA) or poly(2-vinylpyridine) (P2VP), by metal. This differential wetting leads the diffusing metal atoms to aggregate inside domains of the block for which there are favorable, noncovalent polymer/metal interactions. For PS-*b*-P2VP films consisting of hemispherical PS micelles of 150 nm diameter, 9 nm height, and 350 nm lateral spacing in a P2VP matrix, ~5 nm or 29 ML of titanium (Ti) could be thermally evaporated on the diblock copolymer film surface before the preferential accumulation of the Ti on the PS micelles ceased.[78] For PS-*b*-PMMA films comprising cylindrical domains of 50 nm lateral spacing, nearly 100% selectivity of the Ag for the PS domains is observed by transmission electron microscopy (TEM) at an evaporated thickness of 12 nm (42 ML).[51] In the case of a structured monolayer surface consisting of 800-nm-wide DPPC stripes (advancing water contact angle 47 ± 1°) separated by 200-nm-wide mica channels (advancing water contact angle 8 ± 1°), the thermal evaporation of 2−3 nm (7−10 ML) of Ag resulted in a preferential adsorption to the hydrophilic channels.[5,79] It is clear from the step heights measured before and after metal evaporation for DPPC/DLPC that the inherent contrast in the surface energies of the liquid-expanded (~31 mJ m^{-2}) and condensed (~23 mJ m^{-2}) phospholipid phases does not lead to the preferential wetting by metal of the surrounding matrix (LE) versus the stripes (condensed).[80] It is the affinity of the metal for the sulfur that steers the diffusing Au atoms to the surface-exposed disulfide groups of the mixed monolayer. However, once a significant number of the available disulfides have reacted and/or are covered with metal, there is little (or no) physicochemical preference for the incoming metal atoms to deposit on the surface of the metal clusters versus the unfunctionalized phospholipid phase, and the selectivity of the deposition is lost.

PVD of metal under vacuum was employed as a starting point because of its thermal compatibility with organic monolayer films. Alternate technologies such as chemical vapor deposition (CVD) and electroless deposition generally entail harsher conditions (i.e., thermal activation temperatures ≥200 °C for CVD[81] and basic or acidic plating solutions for electroless deposition[82]) that are incompatible with phospholipid LB films. Our work, however, demonstrates that the selective metallization of patterned organic monolayer surfaces via reaction of metal vapor with organosulfur groups is not a viable route to fabricating continuous metal nanostructures. For studies of surface plasmon resonance and electronic transport properties, thicker, continuous metal deposits are generally required.[48,51,83,84] This would involve the selective deposition of at least 10 nm of metal on the DSDPPC or DSDLPC areas of the mixed pattern. In related work with mixed SAMs of different surface reactivity (-SH vs -CH_3) formed by microcontact printing, Mittler et al.[85] found organometallic chemical vapor deposition (OMCVD) to be much more effective in the area-selective deposition and growth of gold layers (~25 nm thick) than thermal evaporation. Future work will thus focus on OMCVD of precursors that decompose/vaporize at $T < 100$ °C under vacuum or atmospheric pressure (i.e., compatibility with the thermally sensitive phospholipid monolayers) and have been shown to deposit on thiol-terminated SAMs, for example, $[(CH_3)_3]PAuCH_3$,[85] Hg,[86] and Al.[81] The use of these chemically differentiated mixed monolayers as primary patterns for the area-selective adsorption of Au and Ag nanoparticles, that are transformable into continuous nanostructures by oxygen plasma treatment, will also be pursued as an avenue to fabricating nanopatterned metal structures.[87]

Conclusions

We have demonstrated the use of alkyl chain-derivatized phospholipids to laterally structure chemical functionalities into striped monolayers formed by the Langmuir−Blodgett transfer of phase-separated binary mixtures from the A/W interface onto solid substrates. By using mixtures of DSDPPC/DLPC or DPPC/DSDLPC, metal-reactive -$SSCH_3$ groups were localized in either the condensed stripe domains or fluid background matrix. The stripe widths could be varied from 150 to 500 nm by changing the phospholipid composition and film transfer pressure. XPS shows that the surface -$SSCH_3$ groups react with vapor-deposited metal atoms to form a metal−thiolate species. The AFM step height and cold detergent extraction results presented are consistent with a preferential adsorption of Au, Ag, and Cu atoms onto the -$SSCH_3$ enriched areas of the stripe patterns at submonolayer coverages of the metal. The chemical reactivity exhibited by the organosulfur-modified phospholipid stripe patterns described in this article make these potentially interesting templates for the fabrication of periodic arrays of solid-supported metal nanostructures.

Acknowledgment. This work was supported by NSERC (Canada), CFI (Canada), FQRNT (Québec), Canada Research Chairs program, and Université de Montréal. N.T gratefully

(78) Spatz, J. P.; Eibeck, P.; Mössmer, S.; Möller, M.; Herzog, T.; Ziemann, P. *Adv. Mater.* **1998**, *10*, 849.
(79) Gleiche, M.; Chi, L.; Gedig, E.; Fuchs, H. *ChemPhysChem* **2001**, *2*, 187.
(80) Berger, C. E. H.; van der Werf, K. O.; Kooyman, R. P. H.; de Grooth, B. G.; Greve, J. *Langmuir* **1995**, *11*, 4188.
(81) Lu, P.; Demirkan, K.; Opila, R. L.; Walker, A. V. *J. Phys. Chem. C* **2008**, *112*, 2091.
(82) Mallory, G. O.; Hajdu, J. B. *Electroless Plating: Fundamentals and Applications*; American Electroplaters and Surface Finishers Society: Orlando, FL.
(83) Xu, Q.; Bao, J.; Capasso, F.; Whitesides, G. M. *Angew. Chem., Int. Ed.* **2006**, *45*, 3631.
(84) Chai, J.; Buriak, J. M. *ACS Nano* **2008**, *2*, 489.
(85) Winter, C.; Weckenmann, U.; Fischer, R. A.; Kashammer, J.; Scheumann, V.; Mittler, S. *Chem. Vap. Depos.* **2000**, *6*, 199.
(86) Aliganga, A. K. A.; Wang, Z.; Mittler, S. *J. Phys. Chem. B* **2004**, *108*, 10949.
(87) Minelli, C.; Hinderling, C.; Heinzelmann, H.; Pugin, R.; Liley, M. *Langmuir* **2005**, *21*, 7080.

acknowledges support from FQRNT (doctoral research scholarship), Faculté des études supérieures et postdoctorales of the Université de Montréal, and Groupe de recherche en technologie des couches minces of the Regroupement québécois sur les matériaux de pointe. We thank Dr. Violeta Toader (CSACS/McGill University) for the synthesis of DSDPPC and DSDLPC.

Supporting Information Available: FEGSEM images of 3:1 DSDPPC/DLPC and DPPC/DLPC monolayers, XPS survey scans of mixed monolayers coated with Au, and AFM images of Au-coated DSDPPC/DLPC after cold detergent extraction. This material is available free of charge via the Internet at http://pubs.acs.org.